Online ISSN: 2981-0396 Print ISSN: 2981-0388

International Journal of Iron & Steel Society of Iran

Journal Homepage: https://journal.issiran.com/

Research Articale

Microstructure and tensile properties of laser welded joints between DP590 and plain low carbon steels

H. Ashrafi *[1], F. Mashayekhi [2]

Faculty of Chemical and Materials Engineering, Shahrood University of Technology, Shahrood, Iran

ARTICLE INFO

Keywords:

Laser welding, Dual phase steel, Microstructure, Hardness, Tensile properties.

Article history:

Received 29 December 2023
Received in revised form 29 January 2023
Accepted 09 March 2024

ABSTRACT

In this study, effect of laser power on the microstructure and tensile properties of dissimilar joints between DP590 steel and AISI 1012 steel were investigated. For this propose, three joints were prepared by laser welding using the laser powers of 400, 450 and 500 W. Results showed the formation of a mixture of Widmanstätten ferrite (WF), polygonal ferrite and ferrite-carbide aggregate in the fusion zone (FZ). Although no trace of martensite phase was detected in the FZ and heat affected zone (HAZ) of the AISI 1012 steel side, but Formation of martensite in the HAZ of the DP590 steel side resulted in the local hardening, while tempering of the pre-existing martensite in the subcritical HAZ of the DP590 steel side led to the formation of a softened zone. Furthermore, the hardness gradually increased from the AISI 1012 steel base metal (BM) to the FZ due to grain refinement and formation of WF. The sample welded with a laser power of 400 W failed from the FZ at early stages of tensile testing due to a lack of penetration defect, while the samples welded with laser powers of 450 and 500 W exhibited ultimate tensile strength values slightly above that of the AISI 1012 steel, and a significantly reduced total elongation value compared to both BMs.

1. Introduction

The rising global energy consumption has led to an increase in fuel prices, which in turn has created a greater demand for fuel-efficient vehicles. Additionally, consumers are now more conscious of the environment and are seeking vehicles that are not only eco-friendly but also provide enhanced safety during accidents. Consequently, the automotive industry has started utilizing advanced high strength steels (AHSSs) to address these conflicting demands [1-3]. AHSSs are being used to reduce the weight of vehicle bodies and closure panels, while simultaneously improving energy absorption in specific areas and stiffness in others. Dual phase (DP) steels are one of the popular groups in the AHSS family, which produced through intercritical annealing followed by rapid cooling. Their microstructure is composed of ~ 10-50 vol.% of martensite islands in the ferrite matrix. Currently, several grades of DP steels are being used in auto-body components such as B-pillars and bumpers [4, 5].

Recently, automotive part manufacturers have become interested in applications of AHSSs in fabrication of tailored welded blanks (TWBs). TWBs are blanks of different materials and/or shapes, grades and thicknesses that are welded together before the stamping operation. This design allows blanks to be made of the most appropriate materials at the right place, leading to weight reduction

*Corresponding author
Email: hashrafi@shahroodut.ac.ir
Address: Faculty of Chemical and Materials Engineering, Shahrood University of Technology, Shahrood, Iran
1. Assistant Professor, 2. Bsc

http://10.22034/IJISSI.2024.2019085.1275
Published by ISSI (Iron & Steel Society of Iran)

and cost minimization [6-9]. Since DP steels have high strength combined with improved ductility, it may be beneficial to use these steels where energy absorption and high strength characteristics are important, while other materials such as mild steels can be used where reduced strength is desired. Laser welding (LW) is widely used in the joining of TWBs, due to its flexibility, high quality, excellent finish and reliability in manufacturing compared with other processes such as gas metal arc welding, gas-tungsten arc welding and electron beam welding [10, 11].

LW of DP steels have been extensively studied in the past decade. Farabi et al. [12] studied tensile properties and work hardening behavior of laser welded DP600 and DP980 steel joints. Bandyopadhyay et al. [13] investigated the formability of laser welded DP steels and reported a decreased formability for laser welded DP600 and DP980 steel welds compared to their respective base metals (BMs). Alves et al. [14] optimized the parameters of LW to minimize the amount of softening in the HAZ of DP1000 steel joints. Parkes et al. [15] evaluated the microstructure and fatigue properties of fiber laser welded joints of DP980 and high strength low alloy steel. Mostaan et al. [16] investigated the effect of silicon content on phase transformation, microstructural evolutions and mechanical behavior of laser welded DP steels. In a recent publication, Ozturk and Arikan [17] studied LW of DP600 to DP800 steel sheets with different thicknesses. They also investigated the effect of laser power and welding speed on the mechanical properties of the TWBs.

The aim of the present work is to investigate the microstructure and tensile properties of laser welded DP590 steel to a plain low carbon steel for use in TWBs. Furthermore, the effect of laser power on the microstructure and tensile properties is also investigated.

2. Materials and methods

1.6 mm thick sheets of DP590 and AISI 1012 steels, with the chemical compositions listed in table 1, were used in this research. Samples with the dimensions of 100 mm × 40 mm were cut from the initial sheets and butt-welded in a dissimilar configuration perpendicular to the rolling direction using a diode laser machine. Table 2. presents the parameters of the LW operations. Before welding, the samples were de-scaled mechanically and cleaned with acetone. Argon gas with a flow rate of 10 L/min was used as the shielding gas during the welding.

Specimens for microstructural analysis were cut from the welds cross-section, mounted, mechanically grounded to 2500 grit finish, polished with a 0.3 μm alumina suspension, and etched with 3% Nital reagent. The microstructure of the etched specimens was studied using optical microscopy (OM). The volume fraction of martensite in the DP590 steel was measured by point counting method based on the ASTM-E562-19 standard [18], using the Image J software. Grain size measurements was carried out by linear intercept method according to the ASTM-E112-13 standard [19].

Microhardness profile of the cross-section of welded samples was measured at a load of 100 g with a dwell time of 10 s using a Vickers microhardness tester (Buehler). In order to determine the tensile properties, uniaxial tensile tests were conducted on the BMs and welded joints perpendicular to the welding direction at a cross-head speed of 1 mm/min using SANTAM STM150 machine. Tensile specimens with the geometry and dimensions shown in Fig. 1. were cut from the BMs and welded samples through electrical discharge machining. The tests were repeated three times to access the average value of tensile properties.

Table 1. Chemical composition (wt.%) of DP590 steel used in this research.

steel	C	Si	Mn	S	P	Cr	Cu	Al	Fe
DP590	0.073	0.32	1.78	0.005	0.024	0.012	0.038	0.04	Bal.
1012	0.12	0.1	0.5	0.026	0.037	-	-	-	Bal.

Table 2. Processing parameters of LW operations.

Sample	Welding speed (mm/min)	Laser power (W)
P400	50	400
P450	50	450
P500	50	500

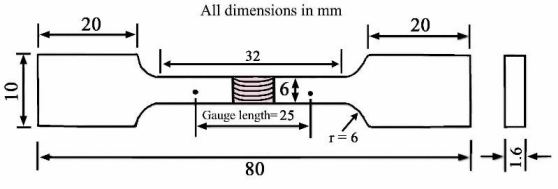

Fig. 1. Geometry and dimensions of the tensile specimens.

3. Results and discussion

3.1. Thermodynamic calculations

Fig. 2. shows the equilibrium weight percentage of phases at different temperatures for the DP590 and AISI 1012 steels obtained by thermodynamic calculations. According to Fig.2a. the solidification of the DP590 steel begins at 1517 °C (liquidus temperature), and ends at 1460 °C (solidus temperature). Austenite is the only stable phase between 1460 °C and 837 °C (A_3). From 837 °C to 680 °C (A_1), ferrite phase is also stable besides austenite. Below 680 °C, ferrite phase with a small amount of cementite coexists. For the AISI 1012 steel (Fig. 2b.), the liquidus and solidus temperatures are respectively 1525 °C and 1455 °C. The A_3 and A_1 are 870 °C and 715 °C, respectively, which both are ~ 35 °C higher than those calculated for the DP590 steel. This means that the temperature range for the stability of austenite phase in the DP590 steel is wider than that in the AISI 1012 steel. This can be attributed to the presence of a higher amount of manganese in the former, as this element promotes the stability of austenite over ferrite [20].

3.2. Macrostructure

Macroscopic image of the welds cross-sections is illustrated in Fig. 3. In the P400 sample, a lack of penetration (LOP) defect was detected, while for the other two samples the weld was sound and free from any defect. Widening of the fusion zone (FZ) with increasing the laser power was another noticeable feature observed in Fig. 3. A schematic illustration of the peak temperature range in different areas of weld cross-section with respect to the iron-carbon phase diagram is shown in Fig. 4. In the FZ (A-A), the peak temperature is above the liquidus temperature of steel, resulting in complete melting. In the uppercritical HAZ (A-B), the peak temperature is above the critical temperatures of A_3, resulting in complete austenitization. This area can be divided into two subzones, coarse grained HAZ (CGHAZ) in which the peak temperature is well-above the A_3 so that the austenite grain growth is noticeable, and fine-grained HAZ (FGHAZ) in which the austenite grain growth is limited. In the intercritical HAZ (ICHAZ), the peak temperature is between A_1 and A_3, resulting in partial austenitization. The peak temperature in the subcritical HAZ (SCHAZ) is below the A_1 (CD), which can have effects like tempering of martensite on the BM. The width of each zone is directly proportional to its temperature range in the iron-carbon phase diagram.

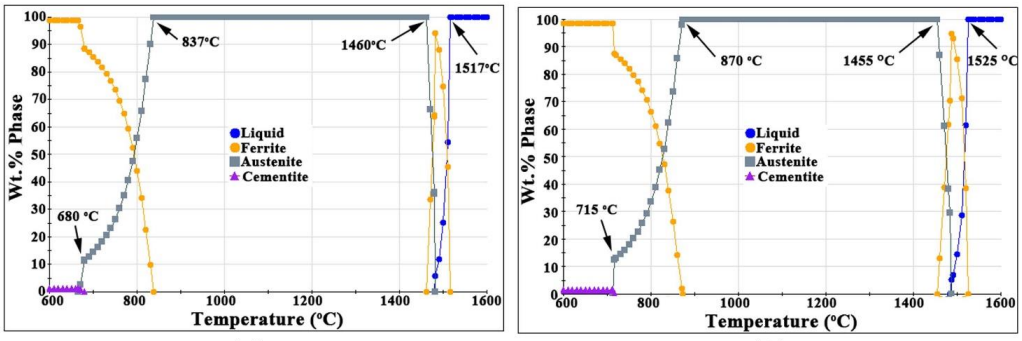

Fig. 2. Equilibrium weight percentage of phases from 600 °C up to the liquidus temperature for (a) DP590 steel, (b) 1012 steel.

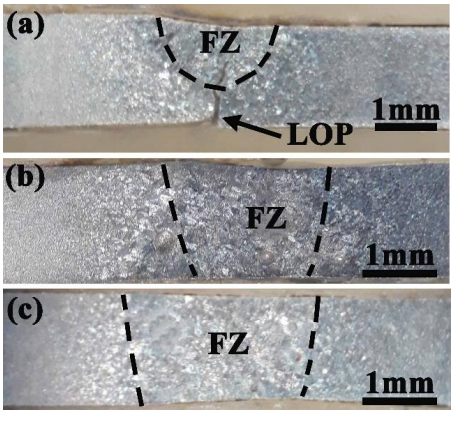

Fig. 3. Macroscopic image of the cross section of different joints: (a) P400, (b) P450, (c) P500.

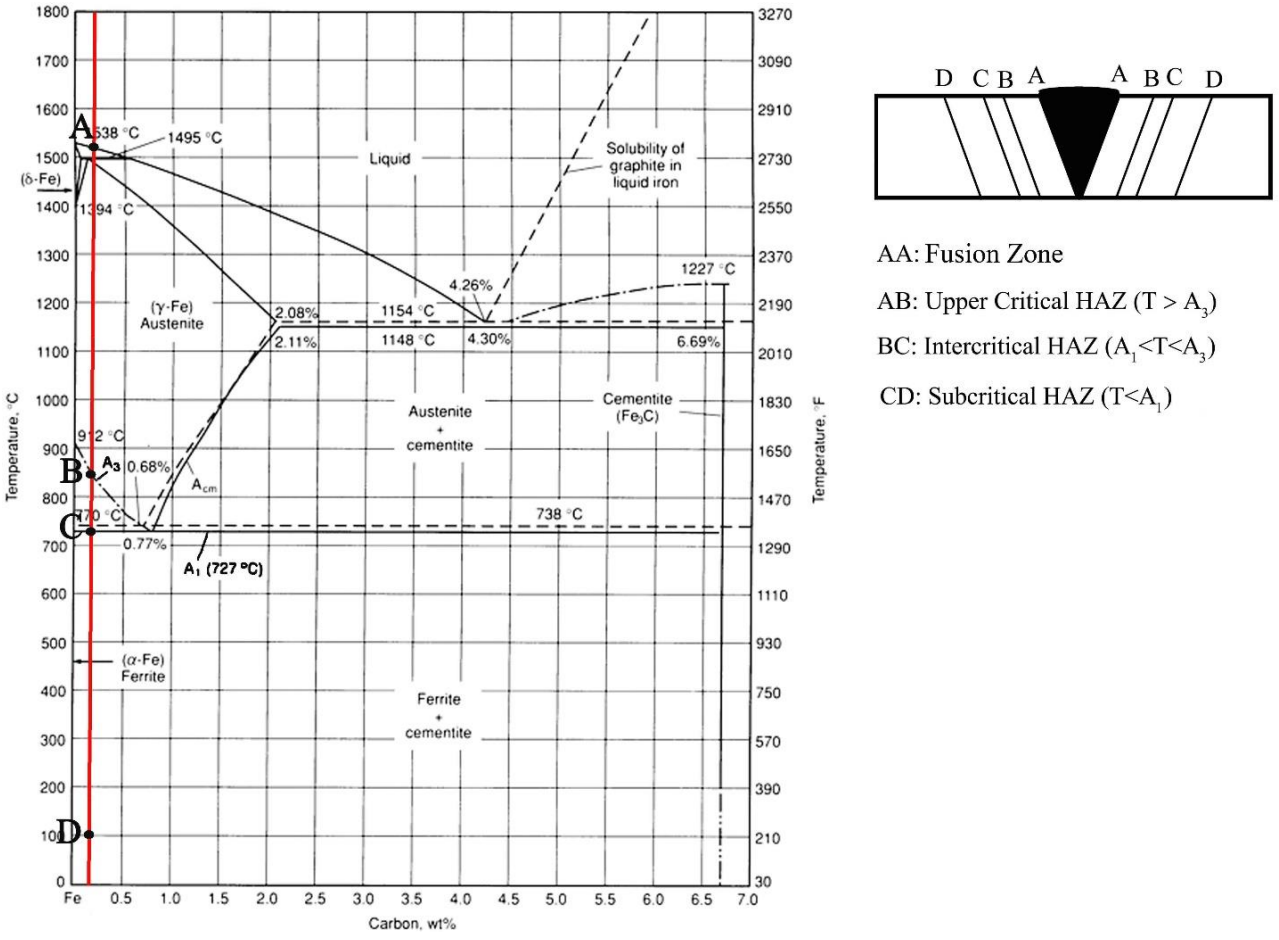

Fig. 4. Schematic illustration of various temperature ranges in the cross-section of a low-carbon steel welded joint.

3.3. Microstructural analysis

Fig. 5. shows OM images of the microstructure of the BMs. As illustrated in Fig. 5a. the microstructure of the DP590 steel was composed of fine martensite islands (dark) mostly distributed in the boundaries of ferrite matrix (light). The mean diameter of martensite islands was ~0.8 µm with a volume fraction of ~22%, and the average grain size of ferrite was ~5 µm. It is demonstrated that presence of very fine martensite islands in ferrite matrix can improve the ductility of DP steels [21]. In the AISI 1012 steel (Fig. 5b.), a completely ferritic microstructure with a mean grain size of ~9 µm was observed.

OM image of the microstructure of the FZ in different samples is shown in Fig. 6. A mixture of Widmanstätten ferrite (WF), polygonal ferrite (PF) and ferrite-carbide aggregate (FCA) was observed in all samples. The latter is composed of a mixture of very fine and spherical cementite particles in a ferrite matrix [22]. No trace of martensite was observed in the FZ, in contrast to previous observations on the LW of DP steels [23, 24]. In the case of autogenous welding, the chemical composition of FZ is ideally the average of the chemical composition of the two BMs. Therefore, the chemical composition of the FZ in the present work can be estimated as: %C = 0.097, %Mn = 1.14, %Si = 0.21. This composition is similar to that of low carbon steels which have a very low hardenability. Therefore, martensite can hardly form in the FZ even at cooling rates as high as what can achieve during LW. This effect of hardenability on the microstructure can better be understand from Fig. 7. which shows the fusion boundary (FB) in the DP590 steel side. It is observed that the microstructure changes from martensite in the CGHAZ of the DP590 steel with a higher hardenability, to ferrite in the FZ with a lower hardenability.

Fig. 8. shows OM images of the microstructure of the CGHAZ in the DP590 steel side. For all samples, a mixture of martensitic, WF and acicular ferrite (AF) were present. Prior austenite grain boundaries (PAGBs) were also detected in Fig. 8. and marked by dashed lines. A comparison between the size of the prior austenite grains in different samples demonstrated that it is increased from ~40 µm to ~90 µm with increasing the LW power from 400 W to 500 W. This is because by increasing the LW power, the time that CGHAZ remains at high temperatures increases. The higher LW power also means a higher welding heat input, resulting in a decreasing cooling rate and promoting the formation of WF and AF besides martensite.

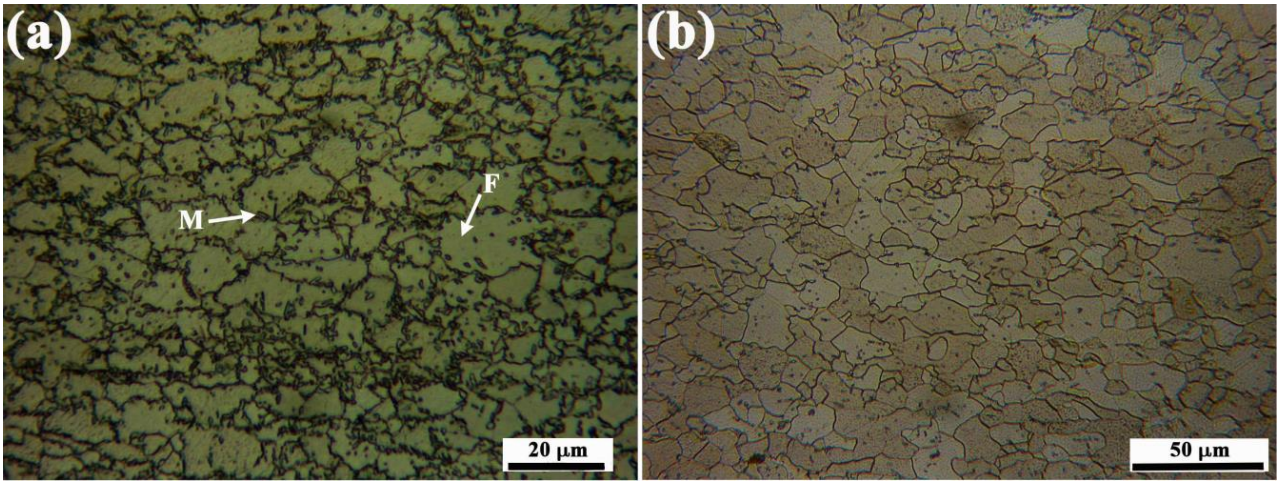

Fig. 5. OM image of the microstructure of (a) DP590 steel, and (b) 1012 steel.

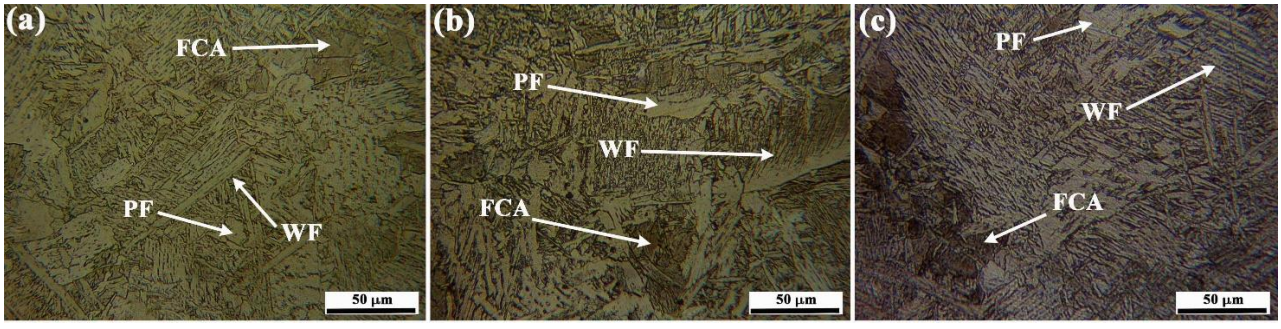

Fig. 6. OM image of the microstructure of the FZ in different samples: (a) P400, (b) P450, (c) P500.

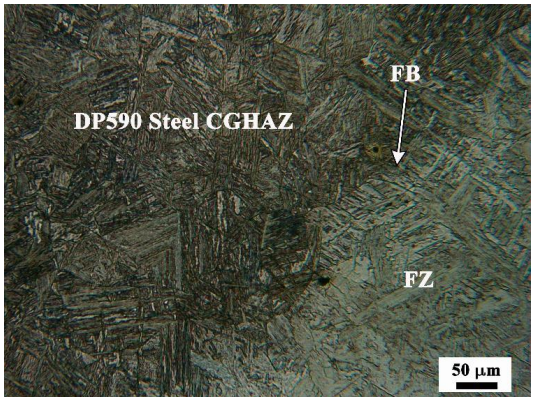

Fig. 7. OM image of the FB in the DP590 steel side.

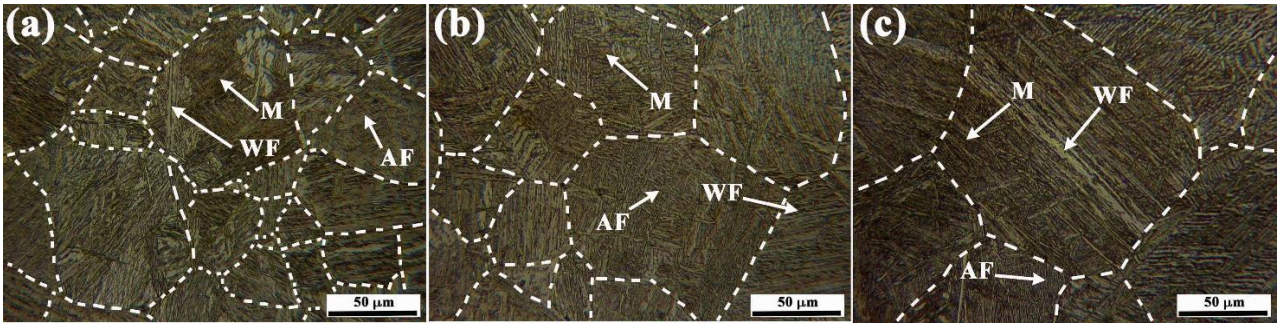

Fig. 8. OM image of the microstructure of the CGHAZ in the DP590 steel side, (a) P400, (b) P450, (c) P500. Dashed lines show PAGBs.

Typical microstructure of the outer part of the HAZ in the DP590 steel side is shown in Fig. 9. In Fig. 9a. the microstructure of a point between the CGHAZ and FGHAZ is also presented. As can be seen, the microstructure in this point was nearly fully martensitic, with fine grains of prior austenite. In the FGHAZ (Fig. 9b.), a mixture of ferrite and martensite was observed. However, the size of ferrite grains (2.7 μm) was smaller than those in the DP590 steel BM. In this area, the peak temperature during the LW is just slightly above the A_3. This result in the austenitization of the microstructure at peak temperature. However, because the time that this area remains above A_3 is very short, carbon diffusion is negligible and therefore the austenite is inhomogeneous in chemical composition. During the cooling cycle, martensite forms at locations with high carbon concentration while areas that are poor in carbon transform to ferrite. In the ICHAZ, which is a narrow zone marked in Fig. 9c. the peak temperature is between the critical temperatures of A_1 and A_3, which leads to partial austenitization. The austenite then transforms to martensite upon cooling to room temperature. In the SCHAZ (Fig. 9d.), the microstructure was similar to that in the BM (Fig. 5a.). The peak temperature in this area is below the A_1, only causing the tempering of the pre-existing martensite. Therefore, no apparent microstructural change can be seen in the OM image.

Fig. 10. shows typical OM microstructures of different locations within the HAZ in the AISI 1012 steel side. In the CGHAZ (Fig. 10a.), the microstructure was composed of a mixture of WF, FCA and PF. In fact, the hardenability of the AISI 1012 steel is not enough to form martensite at cooling rates experienced during the LW. In the FGHAZ (Fig.10b.), ferrite grains with a size significantly reduced compared to that in the AISI 1012 steel (Fig. 5b.), with a small amount of pearlite were observed. In this area, the fine-grained austenite forms at peak temperature transforms to fine-grained ferrite and pearlite, as reducing the grain size of austenite encourages the formation of eutectoid transformation products. The grain size of ferrite increased by moving from FGHAZ to SCHAZ in the ICHAZ (Fig. 10c.). The microstructure in the SCHAZ, as shown in Fig. 10d. was similar to that in the AISI 1012 steel, except the appearance of some pearlite colonies.

3.4. Microhardness measurement

Fig. 11. shows the microhardness profile of the weld cross sections. As expected, the hardness was higher in the DP590 steel side compared to the other side. In the former, local hardening and local softening were observed in the HAZ, similar to previous findings on the LW of DP steels [14-25]. The hardening in the CGHAZ is because of the formation of martensite, while the local softening in the SCHAZ is attributed to the tempering of the pre-existing martensite. According to Fig. 11. the width of the hardened zone increases with increasing the laser power, due to the widening of the FZ and CGHAZ. However, the maximum hardness in the hardened zone was lower for the P450 sample compared with the other two samples. This may be attributed to a lower fraction of martensite in the P450 sample, as martensite is the hardest microconstituent present in the hardened zone. In the AISI 1012 steel side, the hardness gradually increases from BM to the FZ, mainly due to the partial grain refinement and formation of WF.

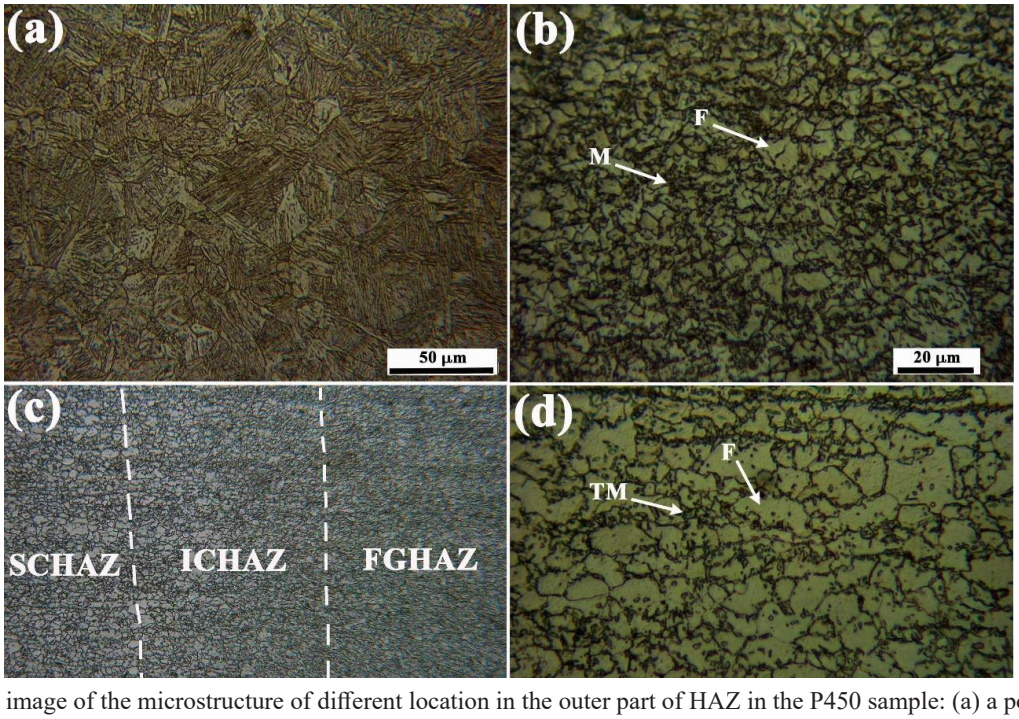

Fig. 9. OM image of the microstructure of different location in the outer part of HAZ in the P450 sample: (a) a point between the FB and SCHAZ (b) FGHAZ, (c) ICHAZ, (d) SCHAZ.

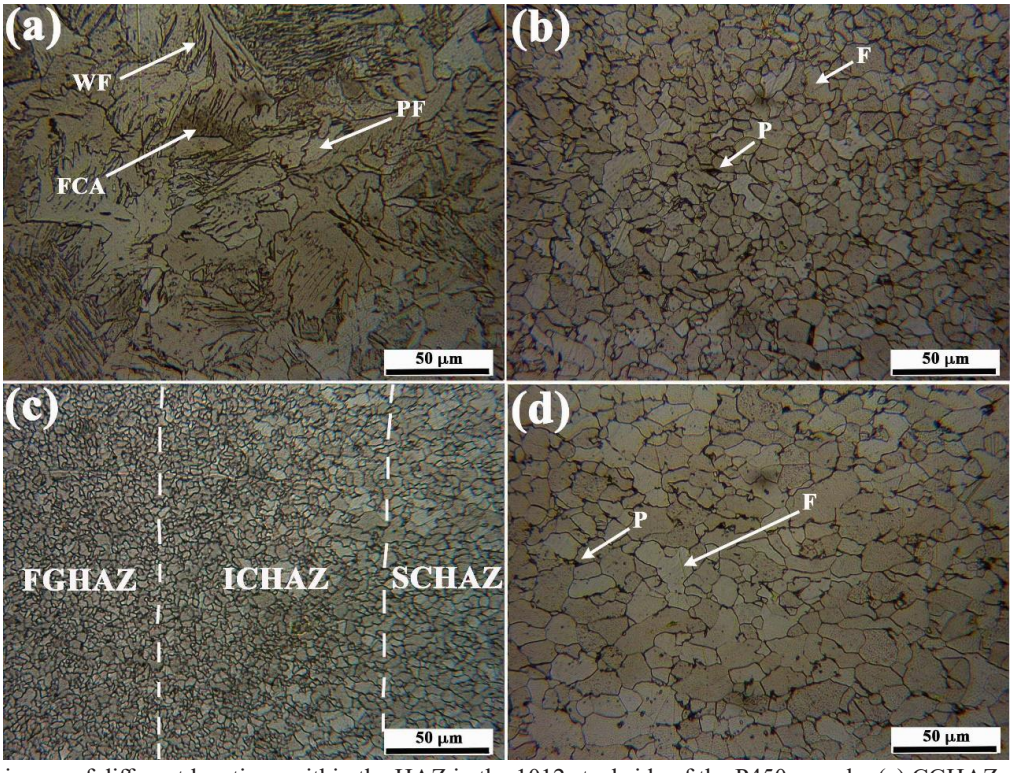

Fig. 10. OM image of different locations within the HAZ in the 1012 steel side of the P450 sample: (a) CGHAZ, (B) FGHAZ, (c) ICHAZ, (d) SCHAZ.

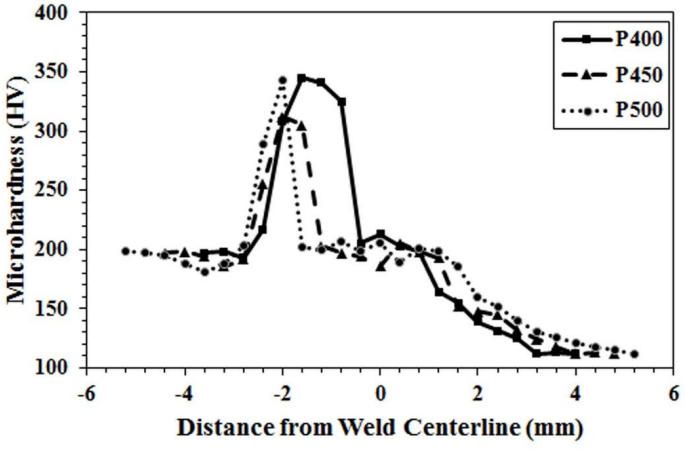

Fig. 11. Microhardness profile of different samples.

3.5. Tensile properties

Fig. 12. shows the representative engineering stress-strain curves of BMs and welded samples. A summary of the tensile properties is also listed in Table 3. The tensile curve of the DP590 steel was indicative of the typical tensile behavior of DP steels, i.e. continuous yielding behavior, low yield strength (YS) to ultimate tensile strength (UTS) ratio and a high elongation [26]. On the other hand, the AISI 1012 steel showed a high elongation over 40% and a discontinuous yielding behavior. The yield point phenomena, which is a result of dislocations locking by interstitial atoms like carbon and nitrogen, is typically observed in the low carbon steels [27]. The P400 sample which had a LOP defect, failed in the elastic region. In the other two welds, the yielding behavior was discontinuous and the UTS as well as elongation were significantly reduced compared to the BMs. However, the YS of both welds were nearly the same as the AISI 1012 steel BM. Analyzing the fractured specimens of the welded samples (Fig. 13.) demonstrated that the fracture location for the P400 sample was in the FZ, while the other two samples failed in the AISI 1012 steel BM. In fact, the significant reduction of elongation in the P450 and P500 samples compared to the BMs was due to the localization of strain in the AISI 1012 steel BM.

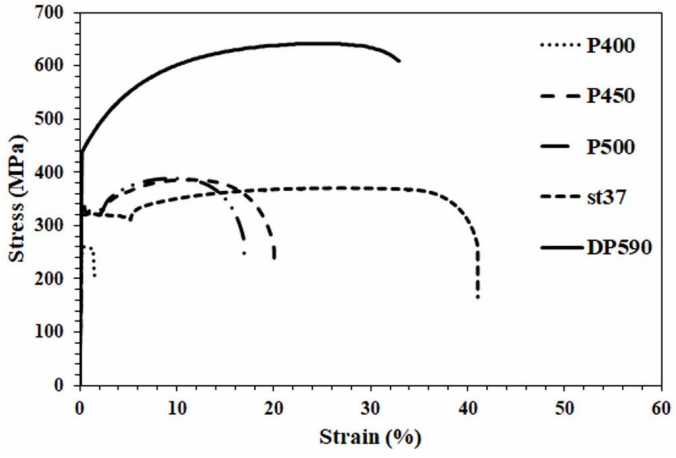

Fig. 12. Engineering stress-strain curves of different samples.

Table 3. Summary of the tensile properties.

Sample	YS (MPa)	UTS (MPa)	Elongation (%)	RA (%)	Fracture location
DP590	438	641	32.9	45.3	-
St37	321	370	41	71.9	-
P400	-	-	-	-	FZ
P450	333	383	20	48.1	st37 steel
P500	338	391	16.95	57.6	st37 steel

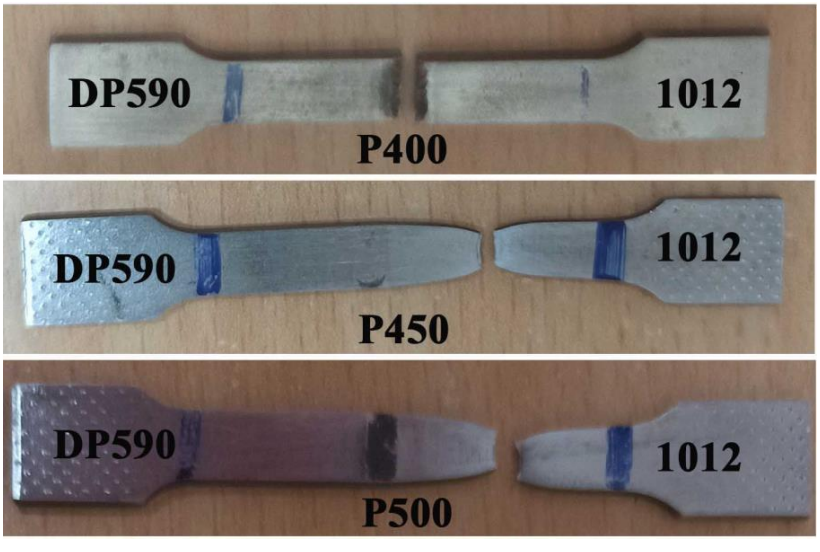

Fig. 13. Macroscopic image of the tensile tested specimens.

4. Conclusions

In this work, effect of LW power on the microstructure and tensile properties of dissimilar joints between DP590 and AISI 1012 steels were investigated. In the sample welded with a power of 400 W, a LOP defect was detected, while sound welds were created using laser powers of 450 and 500 W. The microstructure of FZ in all samples was consisted of a mixture of WF, PF and FCA. No trace of martensite phase was detected in the FZ of all samples. In the CGHAZ and FGHAZ of the DP590 steel side, martensite phase was detected besides ferrite while no trace of martensite was found in the HAZ of the AISI 1012 steel side. Formation of martensite in the HAZ of the DP590 steel side resulted in local hardening, while tempering of the pre-existing

martensite in the SCHAZ of the DP590 side led to local softening. The sample welded with a laser power of 400 W failed from FZ in early stages of tensile test due to the LOP defect, while the other two samples failed from the AISI 1012 steel BM. Furthermore, P450 and P500 samples exhibited YS and UTS values slightly above those for the AISI 1012 steel, with a significant reduction of TE compared to both BMs.

References

[1] Kim J.H, Kim D, Han H.N, Barlat F, Lee M.G, Strain rate dependent tensile behavior of advanced high strength steels: Experiment and constitutive modeling, Mater Sci Eng A. 2013; 559: 222-31.
[2] Khan M.S, Soleymani M, Midawi A.R.H, Aderibigbe I, Zhou Y.N, Biro E, A review on heat affected zone softening of dual-phase steels during laser welding, J Manuf Proc. 2023; 102: 663-84.
[3] Jia Q, Guo W, Peng P, Li M, Zhu Y, Zou G, Microstructure-and strain rate-dependent tensile behavior of fiber laser-welded DP980 steel joint, J Mater Eng Perform. 2016; 25: 668-76.
[4] Anand D, Chen D.L, Bhole S.D, Andreychuk P, Boudreau G, Fatigue behavior of tailor (laser)-welded blanks for automotive applications, Mater Sci Eng A. 2006; 420: 199-207.
[5] Ashrafi H, Shamanian M, Emadi R, Sanayei M, Farhadi F, Szpunar J.A, Characterization of microstructure and microtexture in a cold-rolled and intercritically annealed dual-phase steel, J Mater Eng Perform. 2021; 30: 7306-13.
[6] Panda S, Hernandez V.H.B, Kuntz M.L, Zhou Y, Formability analysis of diode-laser-welded tailored blanks of advanced high-strength steel sheets, Metal Mater Trans A. 2009; 40: 1955-67.
[7] Jia Q, Guo W, Li W, Zhu Y, Peng P, Zou G, Microstructure and tensile behavior of fiber laser-welded blanks of DP600 and DP980 steels, J Mater Proc Technol. 2016; 236: 73-83.
[8] Ahmed E, Reisgen U, Schleser M, Mokrov O, Biaxial behavior of laser welded DP/TRIP steel sheets, Int J Adv Manuf Technol. 2013; 68: 1075–82.
[9] Ashrafi H, Shamanian M, Sanayei M, Farhadi F, Szpunar J.A, The impact of welding heat input on microstructure, micro-texture, and mechanical properties of stir zone in friction stir welded DP600 steel, Mater Today Commun. 2023; 37: 107127.
[10] Sisodia R.P.S, Gáspár M, Draskóczi L, Effect of post-weld heat treatment on microstructure and mechanical properties of DP800 and DP1200 high-strength steel butt-welded joints using diode laser beam welding, Weld World. 2020; 64: 671-8.
[11] Mohammadi Zahrani M, Ranjbarnodeh E, Ketabchi M, Ghassemali E, Microstructure evolution and mechanical properties of laser-welded, joints of 1.2 GPa-class quenching and partitioning steel Opt Laser Technol. 2024; 170: 110257.
[12] Farabi N, Chen D.L, Zhou Y, Tensile properties and work hardening behavior of laser-welded dual-phase steel joints, J Mater Eng Perform. 2012; 21: 222-30.
[13] Bandyopadhyay K, Panda S.K, Saha P, Investigations into the influence of weld zone on formability of fiber laser-welded advanced high strength steel, J Mater Eng Perform. 2014; 23: 1465-79.
[14] Alves P.H.O.M, Lima M.S.F, Raabe D, Sandim H.R.Z, Laser beam welding of dual-phase DP1000 steel, J Mater Proc Technol. 2018; 252: 498-510.
[15] Parkes D. Xu W, Westerbaan D, Nayak S.S, Zhou Y. Goodwin F, et al. Microstructure and fatigue properties of fiber laser welded dissimilar joints between high strength low alloy and dual-phase steels, Mater Des. 2013; 51: 665-75.
[16] Mostaan H, Saeedpour P, Ahmadi H, Nouri A, Laser welding of dual-phase steels with different silicon contents: Phase evolutions, microstructural observations, mechanical properties, and fracture behavior, Mater Sci Eng A. 2021; 811: 140974.
[17] Öztürk E, Arıkan H, Investigation of mechanical properties of laser welded dual-phase steels at macro and micro levels, Opt Laser Technol. 2023; 157: 108713.
[18] Standard Test Method for Determining Volume Fraction by Systematic Manual Point Count, Annual Book of ASTM Standards. 2019; ASTM.
[19]. Standard Test Methods for Determining Average Grain Size. Annual Book of ASTM Standards, 2013: ASTM.
[20] Sun S, Pugh M, Manganese partitioning in dual-phase steel during annealing, Mater Sci Eng A. 2000; 276: 167-74.
[21] Saeidi N, Ashrafizadeh F, Niroumand B, Development of a new ultrafine grained dual phase steel and examination of the effect of grain size on tensile deformation behavior, Mater Sci Eng A. 2014; 599: 145-9.
[22] Ashrafi H, Shamanian M, Emadi R, Sarmadi M.A, Effect of welding parameters on the microstructure and tensile properties of friction stir-welded DP600 steel, SAE Int J Mater Manuf. 2019; 12: 165-78.
[23] Huan P.C, Wang X.N, Yang L, Zheng Z, Hu Z.R, Zhang M, et al. Effect of martensite content on failure behavior of laser welded dual-phase steel joints during deformation, J Mater Eng Perform. 2019; 28: 1801-9.
[24] Jia Q, Guo W, Li W, Peng P, Zhu Y, Zou G, et al. Experimental and numerical study on local mechanical properties and failure analysis of laser welded DP980 steels, Mater Sci Eng A. 2017; 680: 378-87.
[25] Mansur V.M, Mansur R.A.d.F, Carvalho S.M.d, Siqueira R.H.M.d, Lima M.S.F.d. Effect of laser welding on microstructure and mechanical behaviour of dual phase 600 steel sheets, Heliyon, 2021; 7: e08601.

[26] Ashrafi H, Shamanian M, Emadi R, Saeidi N, A novel and simple technique for development of dual phase steels with excellent ductility, Mater Sci Eng A. 2017; 680: 197-202.

[27] Ashrafi H, Shamanian M, Emadi R, Saeidi N, Correlation of tensile properties and strain hardening behavior with martensite volume fraction in dual-phase steels, Trans Indian Inst Met. 2017; 70: 1575–84.